Impact of iron and hydrogen peroxide on membrane degradation for polymer electrolyte membrane water electrolysis

Computational and experimental investigation on fluoride emission

Frensch, Steffen Henrik; Serre, Guillaume ; Fouda-Onana, Frédéric ; Jensen, Henriette Casper; Christensen, Morten Lykkegaard; Simon Araya, Samuel; Kær, Søren Knudsen

Published in:
Journal of Power Sources

DOI (link to publication from Publisher):
10.1016/j.jpowsour.2019.02.076

Publication date:
2019

Document Version
Accepted author manuscript, peer reviewed version

Impact of Iron and Hydrogen Peroxide on Membrane Degradation for Polymer Electrolyte Membrane Water Electrolysis: Computational and Experimental Investigation on Fluoride Emission

Steffen Henrik Frensch[a,*], Guillaume Serre[b], Frédéric Fouda-Onana[b], Henriette Casper Jensen[c], Morten Lykkegaard Christensen[c], Samuel Simon Araya[a], Søren Knudsen Kær[a]

[a] *Aalborg University, Department of Energy Technology, Pontoppidanstræde 111, 9220 Aalborg Øst, Denmark*
[b] *CEA, LITEN, DEHT, F-38054, Grenoble, France*
[c] *Aalborg University, Department of Chemistry and Bioscience, Fredrik Bajers Vej 7, 9220 Aalborg Øst, Denmark*

Abstract

Polymer electrolyte membrane (PEM) degradation in electrolysis mode is simulated through a Fenton model that includes all major involved electrochemical reactions. Supportive experimental investigations on the effect of hydrogen peroxide and iron impurities are carried out in an ex-situ set-up, where the results are utilized to fit model parameters. The experiments reveal a high dependence of fluoride emission on iron concentration, which catalyzes the reaction, and identifies hydrogen peroxide as a necessary precursor for destructive hydroxyl radical formation. Simulations of in-situ operation reveal

* Corresponding author, (+45) 50 25 10 31
Email addresses: stf@et.aau.dk (Steffen Henrik Frensch), guillaume.serre@cea.fr (Guillaume Serre), frederic.fouda-onana@cea.fr (Frédéric Fouda-Onana), hcj@bio.aau.dk (Henriette Casper Jensen), mlc@bio.aau.dk (Morten Lykkegaard Christensen), ssa@et.aau.dk (Samuel Simon Araya), skk@et.aau.dk (Søren Knudsen Kær)

that elevated current is favorable in terms of lower fluoride emission, as the radicals are depleted by side reactions. Temperatures above 80 °C significantly accelerate membrane thinning, where the step from 80 °C to 90 °C more than doubles thinning after 500 h.
Keywords: PEM water electrolysis aging, Membrane degradation modelling, Fenton reaction model, Hydrogen peroxide, Fluoride emission rate

---

Nomenclature

symbol	name	value/ unit
A_i	frequency factor of rxn i	-
$\alpha_{H_2O_2}$	transfer coefficient of rxn 1	0.5
c_s	concentration of species s	$\mathrm{mol\,m^{-3}}$
δ_{mem}	membrane thickness	m
$E_{act,i}$	activation energy of rxn i	$\mathrm{J\,mol^{-1}}$
$\eta_{H_2O_2}$	equilibrium potential of rxn 1	0.695 V
EW	equivalent weight PFSA	$1100\,\mathrm{g\,mol^{-1}}$
F	Faraday constant	$96\,485\,\mathrm{C\,mol^{-1}}$
$f_{F,loss}$	model fit factor	20.8
FER	fluoride emission rate	$\mu\mathrm{g/m^2/h}$
k_i	reaction rate constant of rxn i	$\mathrm{m^3\,mol^{-1}\,s^{-1}}$ (rxn 3 – 13)
$\nu_{F,PFSA}$	partial specific volume PFSA	$\mathrm{m^3\,g^{-1}}$
ω_F	mass fraction of fluorine in PFSA	0.69
R	gas constant	$8.314\,\mathrm{J\,mol^{-1}\,K^{-1}}$
r_i	reaction rate of rxn i	$\mathrm{mol\,m^{-3}\,s^{-1}}$
ρ_{PFSA}	density dry PFSA	$1980\,\mathrm{kg\,m^{-3}}$
T	temperature	K
T^0	reference temperature	298.15 K
υ_s	stoichiometric factor of species s	-
V_s	volumetric flow rate of species s	$\mathrm{mol\,m^{-3}\,s^{-1}}$

1. Introduction

Membrane degradation for polymer electrolyte membrane water electrolysis (PEM WE) is crucial, since it does not only have an impact on cell performance, but also directly affects operation safety. Membrane thinning as a result of degradation increases gas crossover, possibly leading to explosive mixtures [1, 2]. The membrane is therefore considered as one of the lifetime limiting components of a PEM WE system, together with titanium passivation [2]. Membrane degradation in PEM WE is not yet fully understood, but the here described mechanism has been suggested in the literature [2]. Besides protons (H^+) and water (H_2O), also oxygen (O_2) is transported through the membrane from the anode to the cathode side. In the presence of a platinum catalyst, as it is the case in a state of the art PEM WE cathode (CL_c), oxygen and protons react to form hydrogen peroxide (H_2O_2) according to equation I [3]:

$$O_2 + 2H^+ + 2e^- \longrightarrow H_2O_2 \tag{I}$$

In turn, the produced H_2O_2 forms highly reactive hydroxyl radicals ($HO^\bullet$). This reaction is strongly catalyzed by ferrous iron ions (Fe^{2+}) and under that condition well known as the Fenton reaction as seen in equation II:

$$H_2O_2 + Fe^{2+} \longrightarrow Fe^{3+} + HO^\bullet + HO^- \tag{II}$$

The exact mechanisms of the Fenton reaction are not yet fully understood [4], but assumed to play a role in PEM WE degradation. It is commonly agreed that metallic impurities such as iron ions accelerate membrane attack in the presence of H_2O_2. These iron impurities may stem from the balance of plant [2],

however, this claim has yet to be proven and further developed. The assumption is that all components made of stainless steel such as the the cell housing and the piping system release iron ions over time [5]. The behavior of iron within the system is not well documented, i.e. the ions may cross the membrane, stay within it, or be flushed out at one of the outlets. An accumulation of ions would increase the concentration over time, which may affect the reaction kinetics. The radicals formed through the Fenton reaction may attack the membrane structure, which leads to a release of fluoride in the case of Nafion®.

Although the operating conditions and therefore the reaction environment is different in PEM WE, the underlying mechanisms may be deduced from PEM fuel cell (FC) research, since the state of the art membrane material is usually the same. A good PEM FC review can be found in the literature [6] that summarizes the proposal that hydrogen peroxide (H_2O_2) decomposition is highly involved in chemical degradation. This claim is challenged by an experimental investigation, which finds H_2O_2 to be responsible for only a small fraction of membrane degradation [7]. With or without involvement of H_2O_2, radicals may attack the ionomer binder within the catalyst layer, at the interface between catalyst layer and membrane, or diffuse from the cathode electrode back into the membrane, where it can also attack the ionomer. Mitigation strategies include, chemical stabilization of the membrane to limit the number of points of attack, or the implementation of a recombination catalyst layer that prevents oxygen permeation and subsequent H_2O_2 formation [8]. The proposed degradation mechanism may therefore be different for such types of membranes.

A modelling framework for chemical degradation based on radical attack as described above was proposed in [9], who resolved the membrane and assumed the above mentioned involvement of H_2O_2. Similarily, a comprehensive simulation with a focus on radical formation through H_2O_2 compares perfluoroalkyl sulfonic acid (PFSA) membranes to poly(styrenesulfonic acid) (PSSA) membranes and includes an ex-situ Fenton reaction simulation [10]. The authors find very different attack mechanisms for both membrane types and reveal a higher FER for the ex-situ test by 2-3 orders of magnitude. The points of attack and the evolution of their availability in PFSA membranes was simulated by [11], who found a more severe impact of iron ion concentration compared to H_2O_2 on radical formation. Finally, semi-empirical degradation data was incorporated into a model to simulate membrane thinning in [12].

As for PEM WE, a model approach similar to the ones found for PEM FC is described in the literature [13]. The work is based on modelling and experimental data to simulate membrane attack accompanied by membrane thinning. However, the degradation behavior of both are not fully identical [14] and compared to PEM FC, studies dedicated to PEM WE remain scarce. Experimentally, the effect of current density on fluoride emission rate (FER) was investigated in [15], who found a peak between 0.2 and 0.4 $\mathrm{A\,m^{-2}}$. The authors furthermore reported that a majority of membrane degradation can be observed on the cathode side [15, 16], which supports the presented degradation mechanism.

This work aims at developing the presented modelling approach further for PEM WE applications and operation strategies. Furthermore, the simulations are supported by experimental data that investigates the effect of hydro-

gen peroxide and iron ions on fluoride release.

2. Experimental Methodology

For the ex-situ experiment, eleven polypropylene flasks were filled with 100 mL ultra-pure water for the ex-situ experiment. A specific initial concentration of H_2O_2 and Fe^{2+} according to table 1 was established based on preliminary simulations of a realistic cell in operation and a literature review of previous tests [17, 10, 7]. As the exact concentrations in real applications are unknown due to measurement restrictions, the chosen values for the ex-situ investigation can be seen as a sensitivity analysis. The iron concentration was set through iron (II) sulfate heptahydrate ($FeSO_4 \cdot 7\,H_2O$, Merck KGaA) and the hydrogen peroxide concentration through 33%-H_2O_2 solution (VWR Chemicals). 25 cm^2 Nafion® 115 cut into five pieces was immersed and each experiment lasted for 72 h at 80 °C inside an oven. The fluoride content was monitored frequently with an ion selective electrode (ISE, Hach Company ISE301F combined electrode).

For the in-situ tests, the experiments were carried out on a state of the art single cell set-up of 25 cm^2. The MEA was based on a Nafion® 115 membrane, 1.0 $mg\,cm^{-2}$ carbon-supported platinum catalyst layer at the cathode, and 2.3 $mg\,cm^{-2}$ iridium-oxide at the anode. SGL Sigracet® 28BC carbon sheet and a 1 mm titanium sinter with 30% porosity were used as porous transport layers on the cathode and anode, respectively. Purified water was pre-heated and fed to the anode, while the resistivity was monitored at the anode inlet throughout the whole test to ensure a value of 18.2 $M\Omega \cdot cm$. All piping consisted of stainless steel and as the water was not recirculated, no further fil-

ter resin was installed. The fluoride concentration in the effluent water at the cathode and anode outlet was measured through ionic chromatography.

EXP #	$[Fe^{2+}]$ /ppm	$[H_2O_2]$ /wt%
1	0	0
2	1	0
3	1	0.003
4	1	0.03
5	1	0.3
6	1	3
7	1	30
8	0	3
9	0.1	3
10	10	3
11	20	3

Table 1: Experimental matrix for the ex-situ Fenton test. All concentrations refer to their initial value. The highlighted condition is the baseline test

3. Model Development

The degradation processes are assumed to be as described above and depicted in figure 1.

The model approach is carried out in Matlab/Simulink® and consists of a 0-dimensional membrane degradation model, which is implemented into a simple performance model. Membrane degradation is among the most crucial mechanisms for PEM WE and can be considered a lifetime-limiting fac-

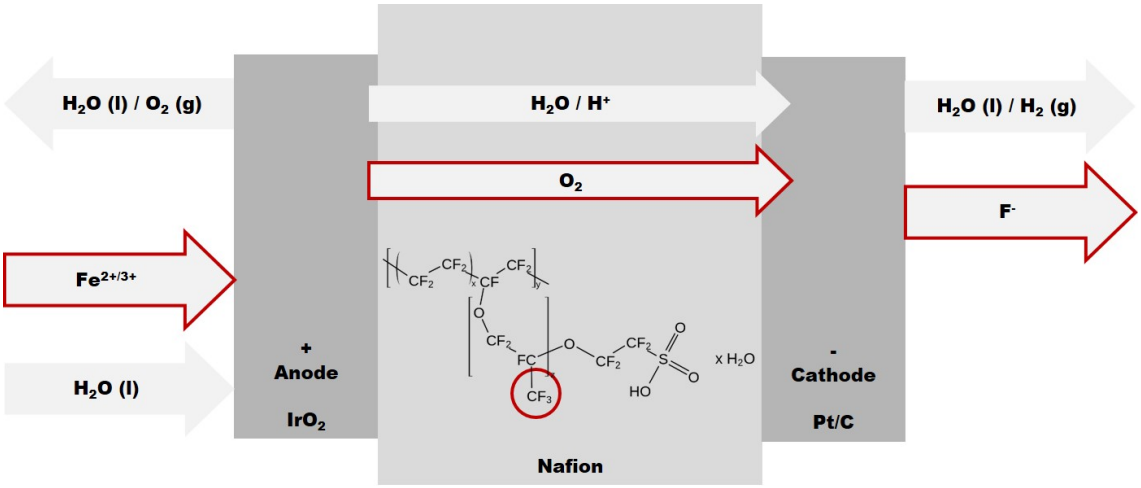

Figure 1: Model scheme for the proposed degradation mechanism

tor [2]. Therefore, capturing the membrane degradation over time through chemical attack is simulated as described above. The Fenton model calculates fluoride emission through concentration of species such as H_2O_2, and the involved radicals. In its core, the description of the involved electrochemical reaction system is based on [13]. In this work, a set of 14 electrochemical reactions was modelled as one reaction system. An overview over the considered reactions is given in table 2.

The main assumptions are:

- all 14 reactions occur in the same space (CL_c)
- oxygen transported to the cathode is entirely and exclusively reduced to hydrogen peroxide (reaction 1)
- reactions 2-13 follow Arrhenius behavior
- the total fluoride emission (reaction 14) as a macroscopic reaction be-

haves like an elementary reaction (i.e. also follows Arrhenius behavior)

3.1. Reaction System and Rate Constants

In a coarse-grained approach, the rate constants at 25 °C and the activation energies for reactions 2 to 13 (except for reactions 7, where data for only one temperature was found) were fitted to the Arrhenius equation as in equation III:

$$k = A \cdot exp(-\frac{E_{act}}{R \cdot T}) \tag{III}$$

where k is the rate constant, A the frequency factor in s^{-1} (also known as the pre-exponential factor), E_{act} the activation energy in $J\,mol^{-1}$, R the gas constant in $J\,mol^{-1}\,K^{-1}$, and T the temperature in K. The rate constant for each reaction was then implemented as a function of temperature. Reaction 1 is implemented as described in section 3.2, while reaction 14 is further addressed in section 3.3. An acidic environment is assumed as the reactions take place close to the highly acidic membrane. The concentrations of species are calculated as in equation IV:

$$\frac{dc_s}{dt} = \sum_{rxn=i} (\upsilon_{s,i} \cdot r_i) + V_{s,in} - V_{s,out} \tag{IV}$$

where υ_s is the stoichiometric factor of species s in reaction i, r_i the reaction rate of reaction i in $mol\,m^{-3}\,s^{-1}$, and $V_{s,in}$ and $V_{s,out}$ the volumetric flow rate of species s in and out of the modelled volume in $mol\,m^{-3}\,s^{-1}$, respectively. The stoichiometric factor is negative for reactants and positive for products by convention. It is furthermore assumed to be zero if the species does not participate in the reaction.

Reaction number	Reaction		E_{act} /kJ mol^{-1}	A /s^{-1}
1	$O_2 + 2H^+ + 2e^-$	$\longrightarrow H_2O_2$	42.45* [13]	-*
2	H_2O_2	$\longrightarrow 2HO^\bullet$	200	$1.09 \cdot 10^{13}$
3	$H_2O_2 + Fe^{2+}$	$\longrightarrow Fe^{3+} + HO^\bullet + HO^-$	35.4	$1.03 \cdot 10^{08}$
4	$H_2O_2 + Fe^{3+}$	$\longrightarrow Fe^{2+} + HOO^\bullet + H^+$	126	$8.31 \cdot 10^{18}$
5	$HO^\bullet + Fe^{2+}$	$\longrightarrow HO^- + Fe^{3+}$	9	$8.68 \cdot 10^{09}$
6	$HO^\bullet + H_2O_2$	$\longrightarrow HOO^\bullet + H_2O$	14	$7.66 \cdot 10^{09}$
7	$HO^\bullet + O_2$	$\longrightarrow HOO^\bullet + H_2O$	-*	-*
8	$HOO^\bullet + Fe^{3+}$	$\longrightarrow Fe^{2+} + O_2 + H^+$	33	$1.21 \cdot 10^{10}$
9	$HOO^\bullet + Fe^{2+} + H^+$	$\longrightarrow Fe^{3+} + H_2O_2$	42	$2.74 \cdot 10^{13}$
10	$HOO^\bullet + H_2O_2$	$\longrightarrow HO^\bullet + H_2O + O_2$	30	$5.41 \cdot 10^{05}$
11	$2\,HOO^\bullet$	$\longrightarrow H_2O_2 + O_2$	20.6	$3.5 \cdot 10^{09}$
12	$HO^\bullet + HO^\bullet$	$\longrightarrow H_2O_2$	7.9	$1.31 \cdot 10^{11}$
13	$HOO^\bullet + HO^\bullet$	$\longrightarrow H_2O + O_2$	14.2	$2.09 \cdot 10^{12}$
14	$HO^\bullet + R_f - CF_2 - COOH$	$\longrightarrow$ products	6.5*	$1.35 \cdot 10^{07}$*

Table 2: Simulated reaction system based on [13]. If not otherwise annotated, the frequency factors were calculated from data for activation energies in [11]. *: For the implementation of reactions 1, 7, and 14, see the respective sections in the text

3.2. Hydrogen Peroxide Formation

Hydrogen peroxide is the precursor of the here considered reaction system, without which no membrane attack would be observed. As described above, the source of H_2O_2 is oxygen that crossed the membrane and is reduced on the Pt catalyst as shown in reaction 1 in table 2. This pathway has been shown to be dominant in a PEM WE cathode environment, while water formation can be neglected [3]. The reaction kinetics are modelled as in equation V [18]:

$$r_1 = k_1 \cdot c_{O_2} \cdot c_{H^+}^2 \tag{V}$$

where c_{O_2} and c_{H^+} are the oxygen and proton concentrations, respectively, and the rate constant k_1 is given as in equation VI [18]:

$$k_1 = k_1^0 \cdot exp(\frac{-E_{act,1}}{R \cdot T}) \cdot exp(\frac{-\alpha_{H_2O_2} \cdot F \cdot \eta_{H_2O_2}}{R \cdot T^0}) \tag{VI}$$

where R, F, and T have their generic meaning, $E_{act,1}$ is the activation energy for reaction 1, and $\alpha_{H_2O_2}$ and η_{H2O2} are the transfer coefficient and equilibrium potential, respectively. k_1^0 is $706.8 \cdot 10^{-14} m^7 \cdot mol^{-2} \cdot s^{-1}$ [18, 13].

While the oxygen concentration is dictated by the dynamics of the reaction system, the proton concentration is dependent on the ionomer humidification and implemented as in equation VII [18]:

$$c_{H+} = \frac{\rho_{PFSA}(\lambda)}{EW} \tag{VII}$$

where $\rho_{PFSA}(\lambda)$ and EW are the humidity-dependent density and the equivalent weight of the ionomer, respectively.

3.3. Membrane Attack Mechanism

The attack mechanism of a polymer such as Nafion® through radicals is widely discussed in the literature [9, 19, 10, 11]. Although the vast majority of publications are attributed to PEM FC, it is assumed that the mechanism itself can be adopted to PEM WE. In this work it is proposed that the radicals formed as described by reactions 2 to 13 attack the ionomer structure at their weak carboxylic acid end-groups (−COOH) [9]. Furthermore, the linkage between backbone and side chains is suspected to be an important point of attack [20, 21].

The attack reaction 14 shown in table 2 is of second order and affected by the concentrations of hydroxyl radicals ($HO^{\bullet}$) and reactive end-groups of the polymer (−COOH). While the $HO^{\bullet}$ concentration is calculated within the reaction system, the concentration of −COOH end-groups is subject of discussion. In this work, a constant value of 200 mM is chosen. This lies within the values found in the literature, where a constant concentration of 1.17M, representing 5% of the total -CF_2- count in the polymer main chain, can be found [10]. The authors interpret this value as an upper limit, while bringing to the attention that a value of around 2 mM to 20 mM would have to be assumed according to [21], with a potential increase over time as described in [20]. A sensitivity analysis of the parameter is carried out below as shown in figure 7. The reaction rate constant k_{14} was not found for any other temperature than room temperature in the literature. Therefore, it is attempted to fit experimental data from the ex-situ experiments to the Arrhenius equation as described later.

3.4. Quantification of Membrane Degradation Through Fluoride Emission

To quantify membrane thinning through fluoride emission, a relationship between fluoride content and membrane volume has to be established. The partial specific volume of the ionomer per unit fluorine can be expressed as in equation VIII [12]:

$$\nu_{F,PFSA} = \frac{1}{\omega_F \cdot \rho_{PFSA}} \tag{VIII}$$

where ω_F is the mass fraction of fluorine within the ionomer, and ρ_{PFSA} is its density. The thinning rate is then expressed as in equation IX [12]:

$$\frac{d\delta_{mem}}{dt} = \nu_{F,PFSA} \cdot FER \cdot f_{F,loss} \tag{IX}$$

where $\nu_{F,PFSA}$ is the above described partial specific ionomer volume, FER the fluoride emission rate as introduced, and $f_{F,loss}$ a factor that accounts for not captured fluoride ions and incompletely decomposed fluorine. It is implemented relative to each captured fluoride ion and therefore technically has the unit $\mathrm{g g^{-1}}$, which means it is dimensionless. The extent of total fluorine emission is not widely reported, but FC research indicates that it might be a considerable share [22]. Therefore, membrane thinning may be underestimated in this approach. On the other hand, all fluoride emission is accounted for membrane thinning, while the ionomer binder in the catalyst layers may also contribute to the total fluoride emission. It is experimentally impractical to differentiate between the origin of fluoride, which may lead to an overestimation of membrane thinning.

4. Results and Discussion

4.1. Ex-situ Fluoride Emission

The fluoride concentration for each experiment over time is shown in figure 2. Experiments with varying initial H_2O_2 concentration are shown in solid lines and varying initial Fe^{2+} concentrations in dashed lines together with the baseline and the pure water test in dash-dot lines.

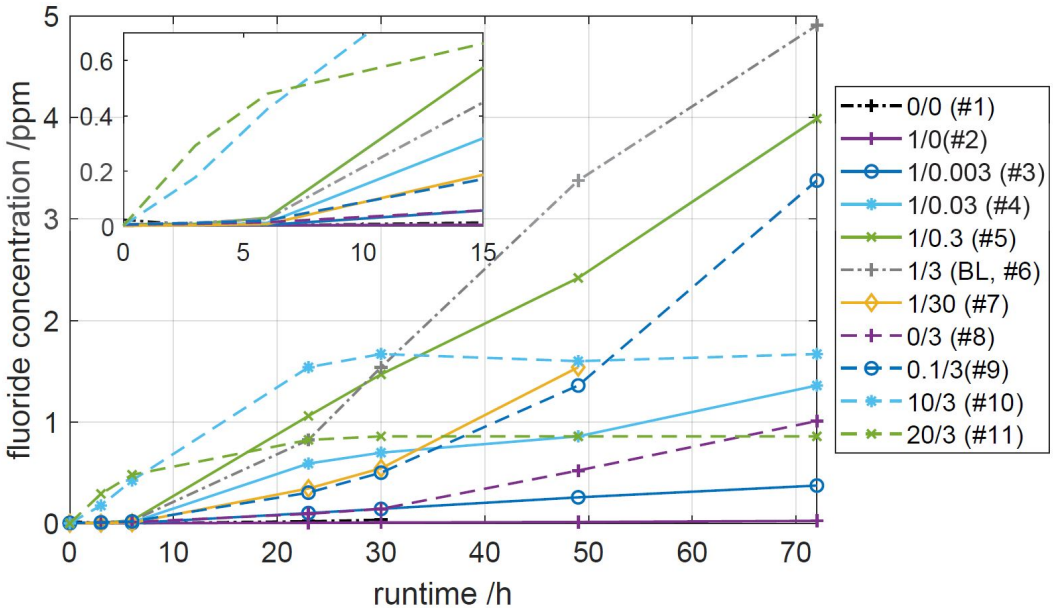

Figure 2: Fluoride concentration over time for all experiments. The legend refers to the initial concentrations as $[Fe^{2+}]/[H_2O_2]$, where BL = baseline test

As expected, the test with neither H_2O_2 nor Fe^{2+} initially (#1) only shows a negligible fluoride release, which might be a consequence of hygrothermal aging [23]. The experiment with no H_2O_2 and 1 ppm Fe^{2+} (#2) also exhibits almost no fluoride emission, while the presence of 3wt% H_2O_2 but no Fe^{2+} (#8) lead to a considerable fluoride concentration especially towards the end of the

experiment of around 1 ppm. This observation supports the above presented assumption that H_2O_2 is as a obligatory precursor for the whole reaction system, while Fe^{2+} acts as a catalyst.

Before analyzing the effect of the initial species concentration in more detail, two different trends can be observed for the reaction kinetics of fluoride emission: Firstly, a steep increase in the first hours, followed by a constant concentration after around 23 h, and secondly, a rate that starts slowly and accelerates over time. The two experiments with high initial Fe^{2+} concentration (#10 and #11) follow the first trend, while all others tend to follow the second. The second category may exhibit an exponential behavior, where experiments with very low initial H_2O_2 concentration (#1, #2, and #3) arguably follow a more linear trend in the investigated time-frame. A longer period of time would have to be investigated in order to conclude on the kinetic trend. For all tests except the ones with high initial Fe^{2+} concentration, the fluoride concentration is below or just around the detection limit of $5 \cdot 10^{-7}$M (= 0.0095 ppm) within the first 3 to 6 hours of test as shown in the magnification in figure 2.

The flattening of the curves with high initial Fe^{2+} concentration is connected to H_2O_2 exhaustion. With Fe^{2+} as a strong catalyst, the initial H_2O_2 may be used up fast with nothing left to run the reaction over a longer time. Therefore, H_2O_2 represent the limiting reactant in these experiments. Consequently, the final fluoride concentration after the test was terminated may be significantly higher if more H_2O_2 was available, either as an initial concentration or as a steady influx. It can in fact be observed, that the highest initial Fe^{2+} concentration of 20 ppm led to highest fluoride emission measured after 3 h as shown in the magnification in figure 2. Possibly due to the same limiting ef-

fect, 10 ppm Fe^{2+} (#10) produced less fluoride emission than 1 ppm Fe^{2+} (#6) after the initial H_2O_2 is completely used up. This appears to be the case after around 30 h. Therefore, a peak appears at 10 ppm after 23 h when plotting the fluoride concentration over initial Fe^{2+} concentration as seen in figure 3a. This peak shifts to 1 ppm after 49 h, when H_2O_2 became limiting for the test at 10 ppm. Therefore, it is expected that a higher Fe^{2+} concentration leads to a higher fluoride emission as long as sufficient H_2O_2 is present.

When looking at the experiment without any initial Fe^{2+} (#8), an unexpectedly high fluoride emission can be observed. Although Fe^{2+} only acts as a catalyst and is theoretically not necessary to produce $HO^{\bullet}$ radicals as shown in reaction 2, simulations of experiment #8 reveal that a fluoride concentration close to zero is expected after 72 h, as can be seen in figure 4b. This discrepancy might be explained by the presence of other metal impurities such as copper ions (Cu^{2+}) in the solution, which catalyze the Fenton reaction but are not implemented in the model [24, 25]. They may stem for example from the membrane manufacturing process or the feed water that may not be purified perfectly. Furthermore, it has been shown in the literature that Fe^{2+} may be replaced by other Fenton-like metal catalysts to produce $HO^{\bullet}$ radicals, including titanium [26, 27]. In the case of a PEM WE cell, titanium is the state of the art material for anodic components such as the bipolar plates. Reactions between other metal impurities and H_2O_2 can be implemented similarly as done with Fe^{2+} in this work.

The impact of initial H_2O_2 concentration on fluoride emission at 1 ppm initial Fe^{2+} concentration can be seen in figure 3b. As for iron, the figure includes measurements after 23 h (blue) and 49 h (red). Besides the above men-

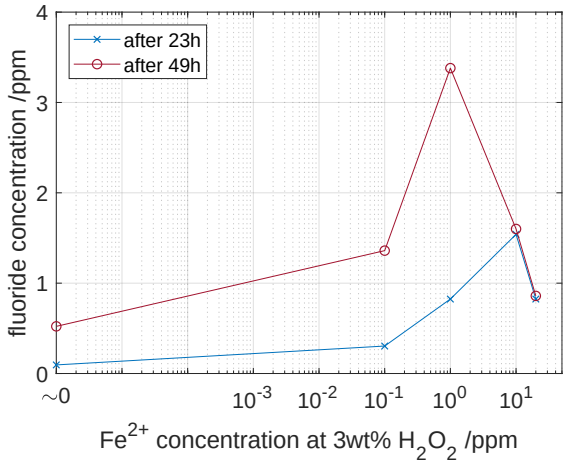

(a) Measured fluoride concentration as a function of initial Fe^{2+} concentration

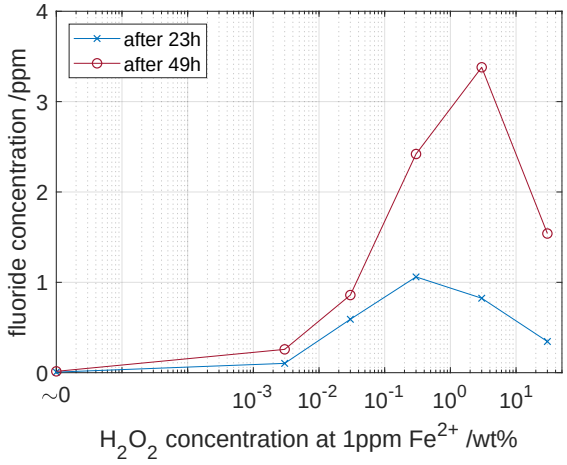

(b) Measured fluoride concentration as a function of initial H_2O_2 concentration

Figure 3: Influence of initial Fe_2^+ and H_2O_2 concentration according to table 2 on fluoride emission

tioned zero-emission at the absence of H_2O_2, a dependency is visible. While low initial H_2O_2 concentration leads to low fluoride emission, the peak is reached between 0.03 and 30wt%, depending on the considered time-frame. This suggests the existence of an optimal concentration to prevent excessive membrane degradation outside these boundaries. Simulations have confirmed the theoretical existence of such an optimum and will be discussed later. In short, the reason is that reaction 6 becomes dominant over the membrane attack reaction 14 at high H_2O_2 concentrations, effectively depleting $HO^{\bullet}$ radicals without fluoride emission. However, intuitively an increase in fluoride emission with H_2O_2 concentration would be expected. A repetition of the set of experiments has to be carried out in order to finally conclude on the existence of an optimum and to rule out experimental errors. An ex-situ experiment was carried out in the literature to find the dependence of the fluoride emission on temperature at 0.36 mM Fe^{2+} (≈ 20 ppm) and 9.68 M H_2O_2 (≈33wt%) [17]. They found a concentration of roughly 0.38 ppm F^- after 9.5 h at 80 °C. The conditions are different from any of the here investigated ones, but come closest to experiment #7 with 30wt% H_2O_2 and 1 ppm Fe^{2+}, where the measured fluoride concentration was 0.35 ppm after 23 h.

4.1.1. Implications on the Membrane Attack Reaction

The model described above is utilized in order to simulate ex-situ behavior and adjusted by setting all in- and outflux to zero. Instead, the initial concentrations of Fe^{2+} and H_2O_2 are set according to the test as in table 1. Furthermore, the initial oxygen concentration was set according to Henry's law due to dilution from the air. The approach is shown for experiment #6 (BL) in figure 4a, while figure 4b compares the measured value to the simulation after

72 h for all tests.

Even though the model estimates correct trends according to the initial conditions, it can be seen that the modelling approach cannot fully capture the kinetics of the reaction. It underestimates fluoride emission with the exception of test #7, #10, and #11. The latter two are highly influenced by H_2O_2 limitation and are therefore excluded from further analysis, although H_2O_2 limitation itself is correctly simulated as a qualitative trend. Experiment #7 with 30wt-% H_2O_2 unexpectedly showed a lower fluoride emission compared to the tests with 3wt-% H_2O_2. As discussed before, this result has to be confirmed and will therefore be excluded for this analysis. Furthermore, experiments #1, #2, and #8 all have simulated emission close to zero and will not be used. Apart from these, the gathered data at 80 °C together with the reported value at 25 °C is utilized to implement k_{14} as a function of temperature to improve model predictions. For that it is assumed that reaction 14 follows the Arrhenius law. Fluoride emission from a polymer membrane has in fact previously been reported to be sensitive to temperature [17].

4.2. In-situ Fluoride Emission

The model inputs for in-situ FER simulations are oxygen crossover, which determines the equilibrium H_2O_2 concentration, and Fe^{2+} influx, which determines the equilibrium Fe^{2+} concentration. Equilibrium concentrations are a result of in- and outflux of species as described in equation IV and appear in an operational cell in steady state. To simulate the impact of both, a baseline for O_2 crossover was set to $6 \cdot 10^{-5} \mathrm{mol\,m^{-2}\,s^{-1}}$, leading to around $= 7.6 \cdot 10^{-3} M$ H_2O_2 equilibrium concentration. This is in fair agreement with the assumed constant background H_2O_2 concentration of $= 5 \cdot 10^{-4} M$ in [10] when con-

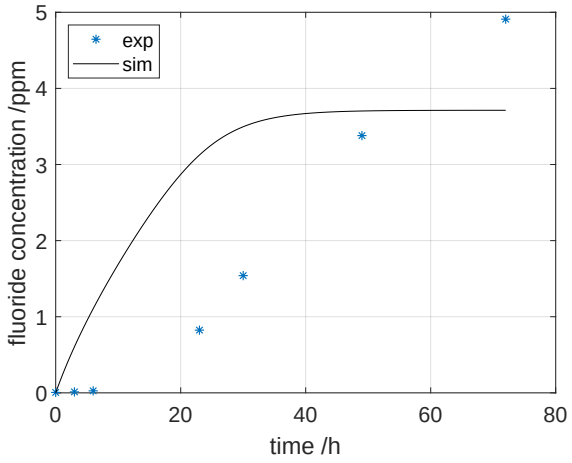

(a) Baseline case (experiment #6, 1 ppm Fe^{2+}/3wt-% H_2O_2)

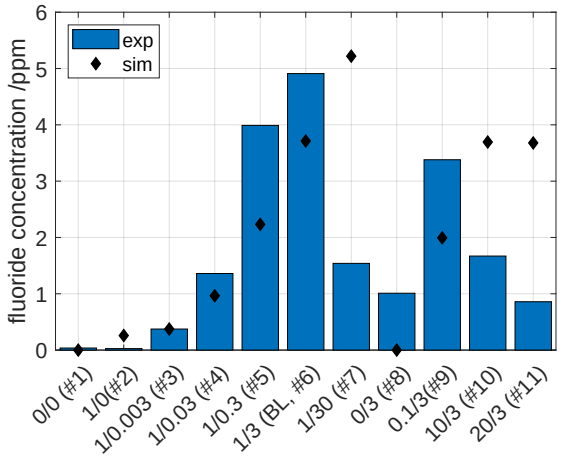

(b) Concentrations as experimentally determined (bars) compared to simulations (⧫) for all experiments. The labels refer to the initial concentrations as $[Fe^{2+}]/[H_2O_2]$, where BL = baseline test

Figure 4: Simulated and measured ex-situ fluoride concentration

sidering that this number will change according to the operation condition. The O_2 permeation rate was found in the literature as experimentally determined at $2.0\,\mathrm{A\,cm^{-2}}$ and 70 °C [28]. The baseline Fe^{2+} influx is set to $3.58 \cdot 10^{-7}\mathrm{mol\,m^{-2}\,s^{-1}}$ (= 1 ppm$\cdot s^{-1}$), leading to $2.6 \cdot 10^{-5} M$ (= 0.13 ppm) equilibrium concentration. The Fe^{2+} influx was chosen as a starting point and is slightly lower than what was found in a previous simulation work [13]. Setting an in- and outflux rather than a constant background concentration assumes that Fe^{2+} has a source term outside the MEA, which might be any stainless steel component in the cell assembly or balance of plant. Lastly, the baseline current was set to $2.0\,\mathrm{A\,cm^{-2}}$ and the temperature to 80 °C.

The model results show that oxygen is needed to produce H_2O_2. H_2O_2 formation is crucial, as it serves as a precursor for all other reactions. This is supported by the ex-situ experiment, where the two tests without H_2O_2 (#1 and #2) lead to a fluoride emission close to zero. The driving force for the membrane attack as in reaction 14 is the $HO^{\bullet}$ radical. Therefore, a lower concentration leads to a lower simulated FER as it can be seen in figure 5. The cause for a lower $HO^{\bullet}$ concentration at higher current can be found within reactions 3, 6, and 7, which are also shown in the figure. While reaction 3 is the dominant pathway for radical production, reactions 6 and 7 are its major sinks besides the attack reaction 14. It can be observed that the reaction rate of reaction 3 decreases with increasing current, whereas the rate for reaction 7 increases due to higher oxygen concentration. As reactions 6 and 7 consume $HO^{\bullet}$ radicals without attacking the ionomer, the fluoride emission is lowered as they become dominant over reaction 14.

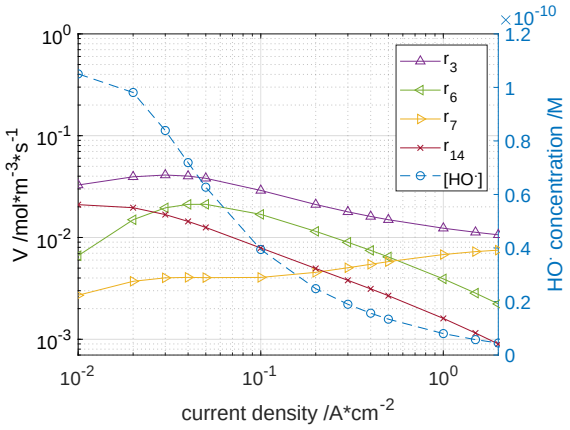

Figure 5: Simulated reaction rates for the most important reactions (left axis) and HO$^\bullet$ concentration (right axis) as a function of current density

4.2.1. Impact of Reactants Influx and Concentrations

The Fe^{2+} influx highly affects the equilibrium concentrations and therefore FER. The simulated effects shown in figure 6a reveal that the equilibrium H_2O_2 concentration is not considerably affected over the majority of simulated range, while a non-linear relationship on equilibrium Fe^{2+} concentration and subsequently FER is visible. This is expected, as reaction 3 produces more HO$^\bullet$ radicals at higher Fe^{2+} concentrations. At very high Fe^{2+} equilibrium concentrations due to a high influx, the FER is decreasing mostly due to a faster depletion of HO$^\bullet$ radicals through reaction 5 as illustrated in figure 6b.

A sensitivity towards O_2 influx can be seen in figure 6c. The simulations reveal that an increase in O_2 influx leads to higher equilibrium concentrations for both O_2 and H_2O_2. Furthermore, it causes a decrease in FER when higher than around $6 \cdot 10^{-6} \mathrm{mol\,m^{-2}\,s^{-1}}$. The dependence lies within reaction 6 and 7, which become dominant over reaction 14 at high H_2O_2 and O_2 concentrations and result in HO$^\bullet$ depletion as shown in figure 5. At the same time, reaction

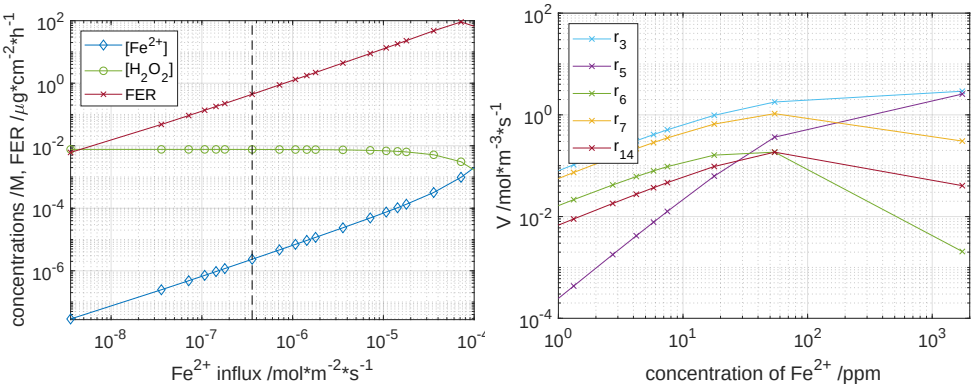

(a) Impact of the Fe^{2+} influx on equilibrium concentrations of Fe^{2+} (dark blue) and H_2O_2 (green), and FER (red)

(b) Impact of Fe^{2+} equilibrium concentration on the most affected reactions

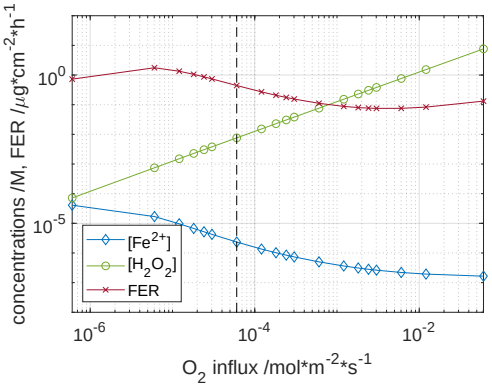

(c) Impact of the O_2 influx on equilibrium concentrations of Fe^{2+} (dark blue) and H_2O_2 (green), and FER (red)

Figure 6: Impact of Fe^{2+} and O_2 on the reaction system. For the other parameters, baseline case is assumed. The baseline influx of the investigated species is marked with the dashed line

9 accelerates slightly, leading to a reduction of Fe^{2+} ions without forming $HO^{\bullet}$ radicals.

Model Sensitivity Towards Reactive End-group Concentration

Unlike the other chemical species, reactive end-groups $-COOH$ do not participate in the reaction system to reach an equilibrium concentration, but are assumed to be constant in this work. As a result of a literature review, the end-group concentration is connected to uncertainty and together with $HO^{\bullet}$, it determines the membrane attack reaction rate. Therefore, the chosen value may affect the accuracy of the simulations and a sensitivity analysis is carried out. The sensitivity study assumed the baseline case. The results are shown in figure 7 and reveal that the FER is in fact changing. A drop of $-COOH$ concentration by one order of magnitude to 20 mM implies a reduction in FER to around one tenth, where an increase by one order of magnitude to 2000 mM roughly increases the FER by a factor of 6.5. Additionally, a higher $-COOH$ concentration amplifies the effect of current on FER. The simulation further reveals that an increase in $-COOH$ concentration shifts the Fe^{2+} equilibrium concentration up by 20%, which may be the cause for the increased FER. End-group concentration has been found to become very limiting on polymer attack below 100 mM under fuel cell conditions, but to remain within the same order of magnitude above [10].

4.2.2. Simulation of a Single Cell and Comparison to in-situ Measurements

In order to simulate a cell in realistic operation, the oxygen influx was implemented as oxygen crossover through the membrane. For this work, the effect of current density on degradation is investigated. Oxygen crossover can be

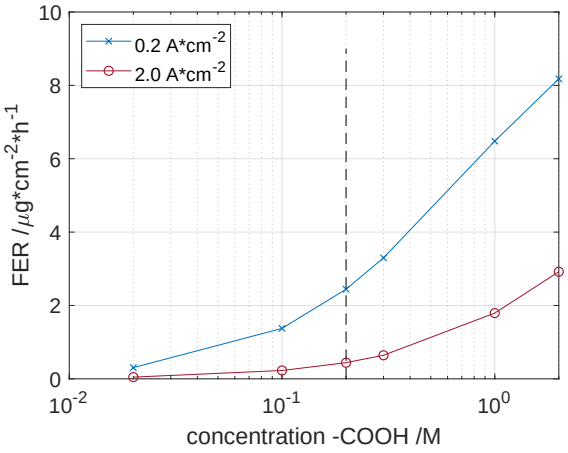

Figure 7: Impact of the concentration of reactive -COOH end-groups on Fe^{2+} concentration (blue) and FER (red). The value used for this work of 200 mM is marked with the dashed line

modelled as diffusion and convection [29], which was experimentally found to be insufficient to describe the behavior [28]. Instead, the oxygen flux at the cathode outlet was found to be a linear function of current density for PEM WE. Although this neglects any potential reactions within the cathode catalyst layer involving oxygen, the crossover is implemented as empirically determined in [28]. Since the experiment was only carried out at 70 °C, the temperature dependence is unknown and not implemented in this approach. The simulated oxygen crossover and FER as a function of current density and temperature can be seen in figure 8a, while the Fe^{2+} influx is set to the baseline case of $3.58 \cdot 10^{-7} \mathrm{mol\,m^{-2}\,s^{-1}}$. Additionally, in-situ measurements at $2.0\,\mathrm{A\,cm^{-2}}$ at 60, 80, and 90 °C are shown.

The simulation reveals that the FER seems to be a negative non-linear function of current density, where higher currents are favorable in terms of minimizing the FER in a real cell application. While running at $0.2\,\mathrm{A\,cm^{-2}}$ at 80 °C

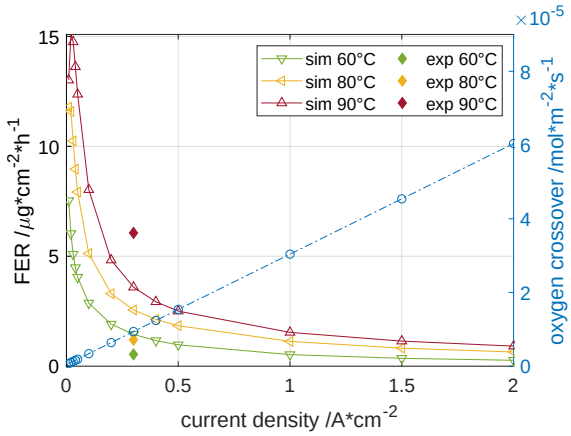

(a) Simulated oxygen crossover from anode to cathode (blue, left axis) and FER at different temperatures (right axis) as a function of current. Additionally, experimental FER at 0.3 A cm^{-2} are shown

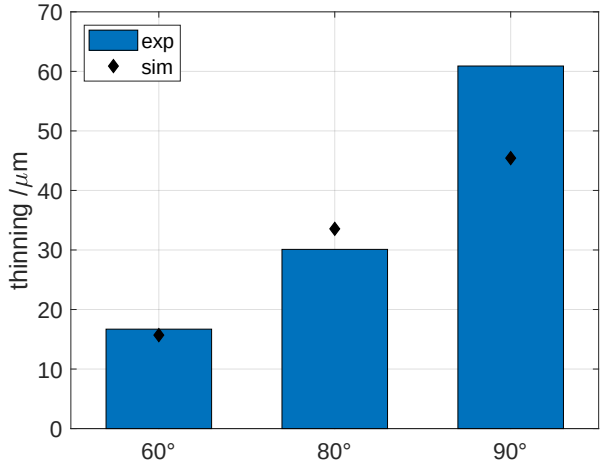

(b) Membrane thinning as determined from SEM images (bars) compared to simulations (⧫)

Figure 8: Comparison of simulations to experimental data from in-situ cells

would lead to a FER of $3.30\,\mu g\,cm^{-2}\,h^{-1}$, operation at $2.0\,A\,cm^{-2}$ lowers that to $0.64\,\mu g\,cm^{-2}\,h^{-1}$. The reason is the decrease in $HO^{\bullet}$ radical concentration at higher currents. This is due to reactions 6 and 7, which deplete radicals faster at higher H_2O_2 and O_2 concentrations, respectively, without attacking the ionomer.

Furthermore, lower temperatures are favorable since they reduce the FER. On the contrary, higher temperatures are generally favorable in terms of performance, which suggests the existence of an optimum operation point when weighing between efficiency and lifetime. However, the simulated effect of temperature is low, especially at increased current density.

The simulation data was compared to data from a previous work, in which FER were measured in-situ on a $25\,cm^2$ set-up at different operation conditions [16]. This experimental data suggested a much bigger dependence of FER on temperature compared to the simulations as it can be seen from the filled diamonds in the respective colors at $0.3\,A\,cm^{-2}$ in figure 8a. The difference in magnitude for all temperatures may be a result of a different Fe^{2+} concentration in a real cell, which is set to the baseline case for the simulation and shown to have a significant impact on FER in figure 6a.

The less pronounced temperature dependence in the experimental data on the other hand can be explained by the model implementation. While the membrane attack (reaction 14) was fitted to the ex-situ results, the oxygen crossover is not implemented as a function of temperature due to the lack of available data. A more sophisticated oxygen generation and transportation throughout the cell has to be implemented in order to compare different operation scenarios. Additionally, the iron influx may be a function of temperature

if assuming corrosion of balance of plant components as a source. Both factors may increase the FER at elevated temperatures. For the sake of completeness, the experimental in-situ data was fitted to the Arrhenius equation, which resulted in 79 kJ mol^{-1} and $4.04 \cdot 10^{18}$ for activation energy and frequency factor for reaction 14, respectively. The activation energy for membrane degradation reaction has previously been reported as around 70 kJ mol^{-1} [10].

4.3. Membrane Thinning Through Fluoride Emission

Membrane thinning was evaluated experimentally in a previous work by means of scanning electron microscopy (SEM) after 500 h for several operation conditions [16]. The values for three temperatures together with the respective simulated thinning according to equation IX is presented in figure 8b. The model fitting factor, $f_{F,loss}$ was set to 20.8 for all simulations [13]. The factor takes into account, that not all fluoride ions are captured in the outlet effluent water. It furthermore accounts for fluorine loss within polymer fragments that cannot be detected by an ion-selective electrode as used in this experimental approach. As a rough estimation, fluorine emission was found up to 6 times higher compared to fluoride [22].

The simulation shows fairly good fit at 60 °C and 80 °C with an error of 6% and 11%, but underestimates thinning at 90 °C by 25%. Given the uncertainties throughout the several assumptions made, these numbers are considered acceptable as a first evaluation of the effect of the operation mode on membrane degradation. Due to the underestimation of fluoride emission at 90 °C, the thinning is also underestimated. As a result, the fitting factor $f_{F,loss}$ could be empirically adjusted to the measured dataset.

Occurrence of membrane thinning and its magnitude has been reported

disputably in the literature. A single cell based on Nafion® 115 and operated at 90 °C was found to have lost 75% of its initial thickness after 5500 h [30]. Two other studies found less, but still perceptible thinning of Nafion® 117 of up to 40% at 80 °C [31, 15]. At a lower temperature of 60 °C, no thinning was observed for Nafion® 115 within a stack after around 700 h [32]. In principle, an important distinction has to be made on whether the polymer has been chemically stabilized or not. Stabilized membranes supposedly exhibit a lower fluoride emission due to their superior chemical durability. However, none of the four above mentioned publications reveal if stabilized or non-stabilized Nafion® was utilized, as both versions exist. While it is fair to assume a non-stabilized product for [31] due to its publication in 1998, no further conclusions can be drawn from the other data. On the other hand, an Aquivion® based cell operated at 55 °C lost around half of its thickness after 3500 h [33]. Although no information on the reported membrane type E098-09 was found, Aquivion® E98-09S only exists as a stabilized version to the authors' best knowledge. A chemical stabilization known as post-fluorination may reduce the amount of available active end groups and therefore lessen membrane thinning.

The here observed thinning rates of around 13% and 23% at 60 °C and 80 °C, respectively, are comparable to the literature. However, the observed rate would lead to an end of life due to increased gas crossover relatively fast, where a commercial system has been reported to operate for 60 000 h [34]. Although they do not report the membrane thinning, the thinning process may be non-linear over time and reduce to a minimum after an initial drop.

5. Conclusion

The influence of hydrogen peroxide and iron ions on fluoride emission have been investigated in ex-situ and in-situ experiments, and through a computational model. The results show that hydrogen peroxide acts as a required precursor, while iron catalyzes the reaction considerably. However, even in the absence of iron, a considerable amount of fluoride emission is observed when H_2O_2 is present. This is linked to the ability of other metallic impurities to replace iron as a catalyzer of the reaction. However, the origin, magnitude, and location of metal impurities have to be identified.

A model based on a system of 14 reactions was developed to simulate ex-situ and in-situ environments. Temperatures above 80 °C as well as low current operation is highly unfavorable in terms of membrane degradation, as the fluoride emission increases non-linearly for both. Furthermore, the simulation revealed high dependence of fluoride emission on reactive end-group concentration, which is a parameter of high uncertainty. Considering the high amount of uncertainties among the developed model, the results are satisfactory for the in-situ simulations for temperatures up to 80 °C when compared to experimental data, but underestimate the effect of temperature above that. This is due to the lack of data for the temperature dependence of oxygen permeation.

Acknowledgement

The authors would like to acknowledge the support by Innovation Fund Denmark through the e-STORE project, Grant 4106-00025B.

References

[1] P. Trinke, B. Bensmann, S. Reichstein, R. Hanke-Rauschenbach, K. Sundmacher, Hydrogen Permeation in PEM Electrolyzer Cells Operated at Asymmetric Pressure Conditions, Journal of The Electrochemical Society 163 (11) (2016) F3164–F3170. doi:10.1149/2.0221611jes.
URL http://jes.ecsdl.org/lookup/doi/10.1149/2.0221611jes

[2] Q. Feng, X. Yuan, G. Liu, B. Wei, Z. Zhang, H. Li, H. Wang, A review of proton exchange membrane water electrolysis on degradation mechanisms and mitigation strategies, Journal of Power Sources 366 (2017) 33–55. doi:10.1016/j.jpowsour.2017.09.006.
URL http://dx.doi.org/10.1016/j.jpowsour.2017.09.006

[3] P. S. Ruvinskiy, A. Bonnefont, C. Pham-Huu, E. R. Savinova, Using ordered carbon nanomaterials for shedding light on the mechanism of the cathodic oxygen reduction reaction, Langmuir 27 (14) (2011) 9018–9027. doi:10.1021/la2006343.

[4] K. Barbusinski, Fenton reaction - Controversy concerning the chemistry, Ecological chemistry and engineering S/Chemia i in{·}zynieria ekologiczna S 16 (3) (2009) 347–358.

[5] A. Pozio, R. F. Silva, M. De Francesco, L. Giorgi, Nafion degradation in PEFCs from end plate iron contamination, Electrochimica Acta 48 (11) (2003) 1543–1549. doi:10.1016/S0013-4686(03)00026-4.

[6] R. Borup, J. Meyers, B. Pivovar, Y. S. Kim, R. Mukundan, N. Garland, D. Myers, M. Wilson, F. Garzon, D. Wood, P. Zelenay, K. More, K. Stroh,

T. Zawodzinski, X. J. Boncella, J. E. Mcgrath, O. M. Inaba, K. Miyatake, M. Hori, K. Ota, Z. Ogumi, S. Miyata, A. Nishikata, Z. Siroma, Y. Uchimoto, K. Yasuda, K.-i. Kimijima, N. Iwashita, Scientific Aspects of Polymer Electrolyte Fuel Cell Durability and Degradation, Chemical Reviews (2007) 3904–3951.

[7] V. O. Mittal, H. Russell Kunz, J. M. Fenton, Is H[sub 2]O[sub 2] Involved in the Membrane Degradation Mechanism in PEMFC?, Electrochemical and Solid-State Letters 9 (6) (2006) A299. doi:10.1149/1.2192696.
URL http://esl.ecsdl.org/cgi/doi/10.1149/1.2192696

[8] D. Bessarabov, A. Kruger, K. Lewinski, Permeation and Recombination of Hydrogen under PEM electrolysis conditions, in: International Conference on Electrolysis, 2017, p. 1.

[9] A. A. Shah, T. R. Ralph, F. C. Walsh, Modeling and Simulation of the Degradation of Perfluorinated Ion-Exchange Membranes in PEM Fuel Cells, Journal of The Electrochemical Society 156 (4) (2009) B465. doi:10.1149/1.3077573.
URL http://jes.ecsdl.org/cgi/doi/10.1149/1.3077573

[10] L. Gubler, S. M. Dockheer, W. H. Koppenol, Radical (HO, H and HOO) Formation and Ionomer Degradation in Polymer Electrolyte Fuel Cells, Journal of The Electrochemical Society 158 (7) (2011) B755. doi:10.1149/1.3581040.
URL http://jes.ecsdl.org/cgi/doi/10.1149/1.3581040

[11] M. Ghelichi, P. E. A. Melchy, M. H. Eikerling, Radically coarse-

grained approach to the modeling of chemical degradation in fuel cell ionomers, Journal of Physical Chemistry B 118 (38) (2014) 11375–11386. doi:10.1021/jp506333p.

[12] M. Chandesris, R. Vincent, L. Guetaz, J.-S. Roch, D. Thoby, M. Quinaud, Membrane degradation in PEM fuel cells: From experimental results to semi-empirical degradation laws, International Journal of Hydrogen Energy 42 (12) (2017) 8139–8149. doi:10.1016/j.ijhydene.2017.02.116. URL http://linkinghub.elsevier.com/retrieve/pii/S0360319917306249

[13] M. Chandesris, V. Médeau, N. Guillet, S. Chelghoum, D. Thoby, F. Fouda-Onana, Membrane degradation in PEM water electrolyzer: Numerical modeling and experimental evidence of the influence of temperature and current density, International Journal of Hydrogen Energy 40 (3) (2015) 1353–1366. doi:10.1016/j.ijhydene.2014.11.111.

[14] H. Liu, F. D. Coms, J. Zhang, H. A. Gasteiger, A. B. Laconti, Chemical degradation: Correlations between electrolyzer and fuel cell findings, in: Polymer Electrolyte Fuel Cell Durability, Springer, 2009, pp. 71–118. doi:10.1007/978-0-387-85536-3_5.

[15] F. Fouda-Onana, M. Chandesris, V. Médeau, S. Chelghoum, D. Thoby, N. Guillet, Investigation on the degradation of MEAs for PEM water electrolysers part I: Effects of testing conditions on MEA performances and membrane properties, International Journal of Hydrogen Energy 41 (2016) 16627–16636. doi:10.1016/j.ijhydene.2016.07.125.

[16] S. H. Frensch, F. Fouda-Onana, G. Serre, D. Thoby, S. S. Araya, S. K. Kær,

Influence of the Operation Mode on PEM Water Electrolysis Degradation. Manuscript submitted for publication (2018).

[17] T. Sugawara, N. Kawashima, T. N. Murakami, Kinetic study of Nafion degradation by Fenton reaction, Journal of Power Sources 196 (5) (2011) 2615–2620. doi:10.1016/j.jpowsour.2010.10.043.
URL http://dx.doi.org/10.1016/j.jpowsour.2010.10.043

[18] V. A. Sethuraman, J. W. Weidner, A. T. Haug, S. Motupally, L. V. Protsailo, Hydrogen Peroxide Formation Rates in a PEMFC Anode and Cathode, Journal of The Electrochemical Society 155 (1) (2008) B50. doi:10.1149/1.2801980.
URL http://jes.ecsdl.org/cgi/doi/10.1149/1.2801980

[19] K. H. Wong, E. Kjeang, Macroscopic In-Situ Modeling of Chemical Membrane Degradation in Polymer Electrolyte Fuel Cells, Journal of the Electrochemical Society 161 (9) (2014) F823–F832. doi:10.1149/2.0031409jes.
URL http://jes.ecsdl.org/cgi/doi/10.1149/2.0031409jes

[20] T. Xie, C. A. Hayden, A kinetic model for the chemical degradation of perfluorinated sulfonic acid ionomers: Weak end groups versus side chain cleavage, Polymer 48 (19) (2007) 5497–5506. doi:10.1016/j.polymer.2007.07.043.
URL http://dx.doi.org/10.1016/j.polymer.2007.07.043

[21] C. Zhou, M. A. Guerra, Z. M. Qiu, T. A. Zawodzinski, D. A. Schiraldi, Chemical durability studies of perfluorinated sulfonic acid polymers and

model compounds under mimic fuel cell conditions, Macromolecules 40 (24) (2007) 8695–8707. doi:10.1021/ma071603z.

[22] M. Bodner, B. Marius, A. Schenk, V. Hacker, Determining the Total Fluorine Emission Rate in Polymer Electrolyte Fuel Cell Effluent Water, ECS Transactions 80 (8) (2017) 559–563.

[23] F. M. Collette, C. Lorentz, G. Gebel, F. Thominette, Hygrothermal aging of Nafion®, Journal of Membrane Science 330 (1-2) (2009) 21–29. doi:10.1016/j.memsci.2008.11.048.

[24] A. B. LaConti, M. Hamdan, R. C. McDonald, Mechanisms of membrane degradation, in: Handbook of Fuel Cells: Fundamentals, Technology, and Applications, John Wiley and Sons, 2003, pp. 647–663.

[25] M. Inaba, Degradation Mechanism of Polymer Electrolyte Fuel Cells, 14th International Conference on the Properties of Water and Steam in Kyoto (2004) 395–402.

[26] S. GOLDSTEIN, D. MEYERSTEIN, G. CZAPSKI, THE FENTON REAGENTS, Free Radical Biology & Medicine 15 (Ii) (1993) 435–445.

[27] Z. Liu, T. Wang, X. Yu, Z. Geng, Y. Sang, H. Liu, In situ alternative switching between Ti ⁴⁺ and Ti ³⁺ driven by H ₂ O ₂ in TiO ₂ nanostructures: mechanism of pseudo-Fenton reaction, Materials Chemistry Frontiers 1 (10) (2017) 1989–1994. doi:10.1039/C7QM00163K.
URL http://xlink.rsc.org/?DOI=C7QM00163K

[28] P. Trinke, B. Bensmann, R. Hanke-Rauschenbach, Experimental evidence of increasing oxygen crossover with increasing current density during PEM water electrolysis, Electrochemistry Communications 82 (June) (2017) 98–102. doi:10.1016/j.elecom.2017.07.018.
URL http://dx.doi.org/10.1016/j.elecom.2017.07.018

[29] P. Olivier, C. Bourasseau, P. B. Bouamama, Low-temperature electrolysis system modelling: A review, Renewable and Sustainable Energy Reviews 78 (March) (2017) 280–300. doi:10.1016/j.rser.2017.03.099.

[30] S. A. Grigoriev, K. Dzhus, D. G. Bessarabov, P. Millet, Failure of PEM water electrolysis cells: Case study involving anode dissolution and membrane thinning, International Journal of Hydrogen Energy 39 (35) (2014) 1–7. doi:10.1016/j.ijhydene.2014.05.043.
URL http://linkinghub.elsevier.com/retrieve/pii/S0360319914013913

[31] S. Stucki, G. G. Scherer, S. Schlagowski, E. Fischer, PEM water electrolysers: evidence for membrane failure in 100 kW demonstration plants, Journal of Applied Electrochemistry 28 (10) (1998) 1041–1049. doi:10.1023/A:1003477305336.

[32] P. Lettenmeier, R. Wang, R. Abouatallah, S. Helmly, T. Morawietz, R. Hiesgen, S. Kolb, F. Burggraf, J. Kallo, A. S. Gago, K. A. Friedrich, Durable Membrane Electrode Assemblies for Proton Exchange Membrane Electrolyzer Systems Operating at High Current Densities, Electrochimica Acta 210 (2016) 502–511. doi:10.1016/j.electacta.2016.04.164.
URL http://dx.doi.org/10.1016/j.electacta.2016.04.164

[33] S. Siracusano, N. Van Dijk, R. Backhouse, L. Merlo, V. Baglio, A. Arico, Degradation issues of PEM electrolysis MEAs, Renewable Energy 123 (2018) 52–57. doi:10.1016/j.renene.2018.02.024.
URLhttp://linkinghub.elsevier.com/retrieve/pii/S0960148118301678

[34] E. Anderson, K. Ayers, C. Capuano, R & D Focus Areas Based on 60 , 000 hr Life PEM Water Electrolysis Stack Experience p Proton OnSite Manufacturer of packaged products , systems, in: First International Workshop on Durability and Degradation Issues in PEM Electrolysis Cells and its Components, 2013, pp. 1–21.